Control of Track Morphology in Digital Glass Forming

Nicholas Capps[a], Jonathan Goldstein[b], Robert Landers[a], Edward Kinzel[a, *]
[a]Aerospace and Mechanical Engineering, University of Notre Dame, Notre Dame, IN, 46556
[b]Air Force Research Laboratory, Wright-Patterson AFB, OH 45433
[*]ekinzel@nd.edu

ABSTRACT

Digital Glass Forming involves locally heating a glass filament using a laser while continuously feeding relative to the workpiece. This enables precise control of the viscosity of the molten region. This viscous melt pool is deformed by forces from the filament and workpiece. This paper investigates the relationships between the input parameters, laser power, feed rate, and scan speed, with the resulting track morphology. Tracks are used to build larger, more complex structures. By underfeeding the filament relative to the able scan speed, the glass is locally drawn to produce tracks with significantly smaller cross-sectional areas than the feedstock material. This technique allows for the production of arbitrary geometries and surface features using a smaller equivalent diameter than the input feedstock. The paper explores the available process zone for this underfed deposition mode and the limitations of this method.

Keywords: Additive manufacturing, Glass

1. Introduction

Silicate-based glasses are attractive materials for structural, scientific, and optical components due to the material's unique combination of material properties. These properties include transparency from the near UV to near IR wavelengths, high thermal stability at elevated temperatures, stiffness, scratch resistance and formability at high temperatures, and the ability to dope the material to change its optical and chemical properties [1-2]. There has been considerable interest in utilizing additive manufacturing (AM) techniques to create optical and structural components from silica-based glasses. However, the material's high molten viscosity and transparency to common laser wavelengths pose a challenge to most common AM methods. There are significant difficulties with bubble evacuation within powder-based approaches, leading to mechanically weak, low transmission parts [3]. There have been some successful methods for creating transparent glass structures, such as a composite method using silica precursor-loaded polymer slurries deposited using conventional approaches such as direct ink writing or stereolithography. These parts are then dried, pyrolyzed and densified following ceramic processing techniques to produce dense 3D glass structures. However, there are challenges to utilizing this method for creating parts with high aspect ratios due to limited build volume and part shrinkage, and the method also suffers from low cycle time [4-6]. Other methods use a traditional fused filament fabrication (FFF) approach to deposit glasses but utilize specialized tooling or alternative feedstock chemical compositions (e.g., chalcogenide) to overcome the high temperature requirements for glass deposition [7-8].

Another glass AM methodology utilizes a CO_2 laser to locally heat solid silica glass feedstocks to deposit the material directly onto a substrate of the same material [9-11]. This method takes inspiration from traditional artisan glass working through the localized application of heating and force to form the feedstock into a bead track, building into the desired shape. By articulating the workpiece using CNC-controlled stages, the mechanical freedom of the artisan can be replicated while significantly improving the resolution, leading to the development of the Digital Glass Forming (DGF) process. Using this method, complex 3D artifacts can be created, ranging from fully dense optical forms to sparse free-standing structures, including lattices, using feedstocks ranging from 3 mm to 125µm OD [11 - 13]. However, the piece's form accuracy is limited by this feedstock material's input diameter. While using a 125µm feedstock will allow for high spatial resolution, the surface resolution required for producing optics is significantly smaller than this [14]. This paper aims to explore a technique of underfeeding the filament relative to the table scan rate to locally draw the filament to a smaller equivalent diameter.

2. Experimental Setup

Figure 1 depicts the DGF setup used in this paper. As shown, 2 mm OD borosilicate feedstock (Duran) is fed into the intersection between a CO_2 laser beam (Iradion 1625, λ_0=10.6 µm) and a borosilicate substrate. Silicate glasses are highly absorptive at 10.6 µm, so the laser power (P) is approximated as surface a heat flux applied to both the feedstock and the illuminated area on the substrate [15]. For all experiments in this paper, the laser spot size

was selected to be 2 mm FWHM. The substrate is mounted to a four-axis positioning system using computer-controlled stages (Aerotech ANT130XY, ATZ100, and ANT130R). The filament is deposited onto the substrate by feeding in the feedstock at feed rate f while translating the work piece at rate v. The filament is oriented at $\theta_F = 40°$ from the substrate normal, while the laser is incident at $\theta_L = 60°$. The system is aligned such that the lines that define the filament's front surface, the substrate's top surface, and the center of the laser spot intersect at the same point. This orientation is selected such that the laser energy is directly delivered to the interface between the filament and substrate, increasing the linear deposition rates of glass and allowing for control of the resulting track morphology via loading from the filament feeder, which will be discussed below [16]. Due to the large thermal gradients generated in the process, deposited pieces are subject to residual stress upon cooling. To prevent thermal shock and cracking of the substrate, the built plate is maintained at 550°C (above the annealing temperature for borosilicate glass) [17].

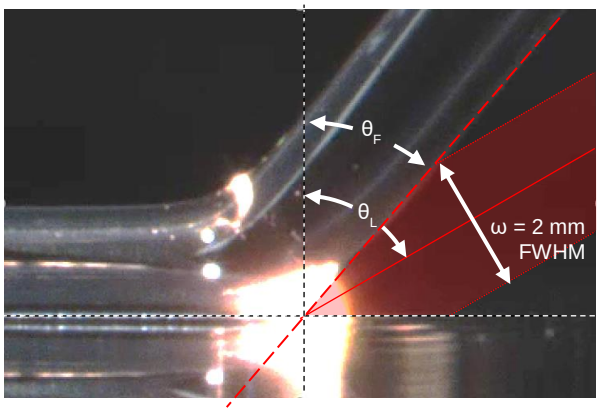

Figure 1: Photograph of the DGF deposition method

Reducing glass feedstock diameters is a common procedure for glass materials, highlighting the unique features of working with glass. While most processes for reducing feedstock diameters to very small equivalent diameters involve pushing molten material through an extrusion nozzle, due to molten glass' very high molten viscosity and temperature requirements, this method is limited to producing filaments diameters ≥ 2 mm [18]. The most common method for producing glass fibers is drawing the material down from a larger feedstock by continuously pulling on the molten glass, using the viscosity and surface tension to maintain the circular morphology [19]. Taking inspiration from the fiber-pulling techniques, we can underfeed the feedstock material (f) relative to the table scan rate (v), pulling on the filament and locally drawing the equivalent diameter down. By conservation of volume, the equivalent radius change of the track compared to the feedstock is related to the ratio of these two velocities by $R/R_0 = (f/v)^2$. For this paper, we arbitrarily chose that the target would be to reduce the 2 mm feedstock diameter down to an equivalent diameter of 0.5 mm, resulting in a target f/v=1/16. There are diminishing returns on f/v shift to equivalent diameter change beyond this point.

Initial experiments with this aggressive underfeeding target showed the most prominent failure mode appeared as the filaments lifting off the substrate, bending in open air. This failure mode can be understood conceptually by examining a simplified force balance model shown in Fig 2 below. In the nominal case at f/v=1 (Left), the primary force delivered to the melt pool is from the filament feeder delivered by the relatively cool back surface of the filament. This is resisted by the normal force of the substrate as well as the viscoelastic deformation of the rest of the filament. Additionally, there are more difficult to define forces such as those supplied by the table scanning as well as surface tension between the filament and substrate. As the table scan rate increases and the filament lifts off the substrate, several of these forces disappear (surface tension and substrate normal force). Instead, the force applied by the stage movement is significantly higher along with a significantly higher viscoelastic deformation component as the filament stretches to the desired length to achieve f/v. Developing a mathematical model to describe these forces and their application is a significant challenge, so an effort was made to empirically define the relationships between the input parameters and resulting morphology. As such an experiment plan was developed to examine the limitations of this approach and identify how close to the f/v target could be achieved.

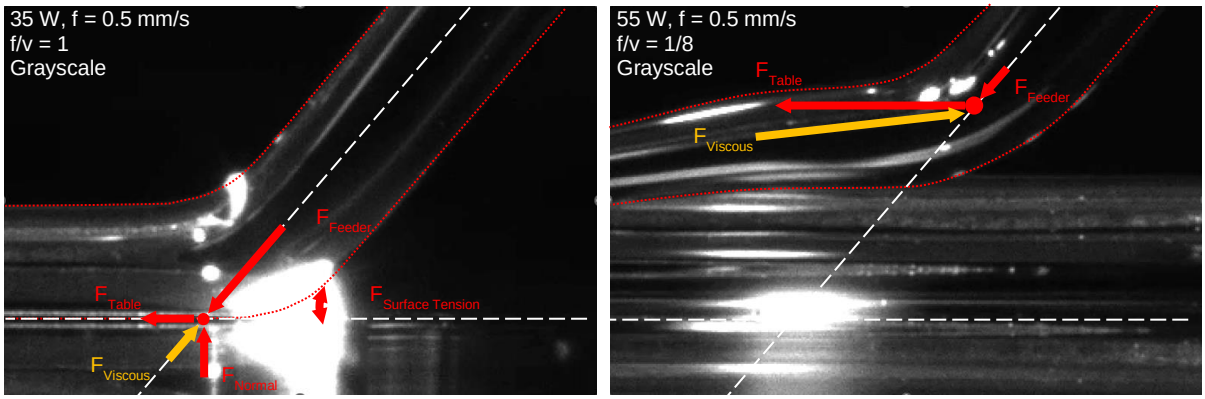

Figure 2: Comparison of force balance of normal and underfed depositions

A parameter sweep was set up to explore the process zone. For this experiment, a static feed rate *f* and laser power were set for each experiment. Table scan speed *v* was then swept to achieve the desired *f/v* ratio. To increase the data throughput per experiment, the feed rate was varied linearly along the length of the deposition of a straight line, as shown in Fig 3 below. The sample was then sectioned along the dashed red lines such that the cross-section at the end of each section could be viewed. For this experiment set, the valid track morphologies were divided into two groups depending on the contact angle (θ_c). To produce fully dense geometries $\theta_c \leq 90°$ (termed as slumped) are desired, while tracks that are attached to the substrate but would result in inter-track voids $\theta_c \geq 90°$ are not. The filled-out process zones for this experiment are shown in Fig 4 below. As shown, in this configuration, the process deposition region is limited to a minimum $f/v \geq \sim 0.2$, due to the presence of this liftoff mode. Notably, the feed rate that maintained the largest viable process zone is at f = 0.5 mm/s, while both higher and lower feed rates had significantly smaller process zones. The effect of feed rate on the process will be discussed in a later section.

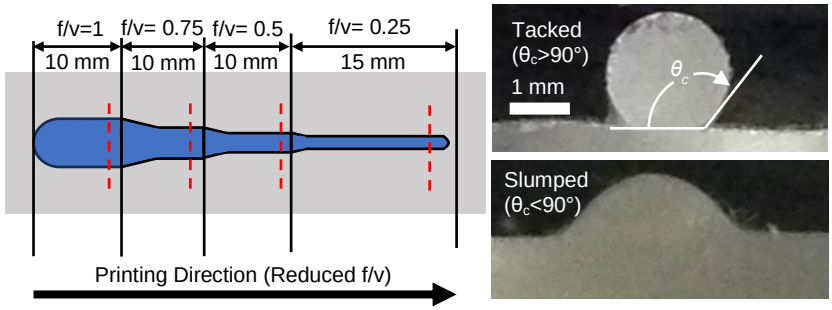

Figure 3: (Left) Diagram of the experimental method, where the track *f/v* ratio decreases linearly from left to right in defined increments. (Right) example cross-sections of filaments based on the resulting contact angle.

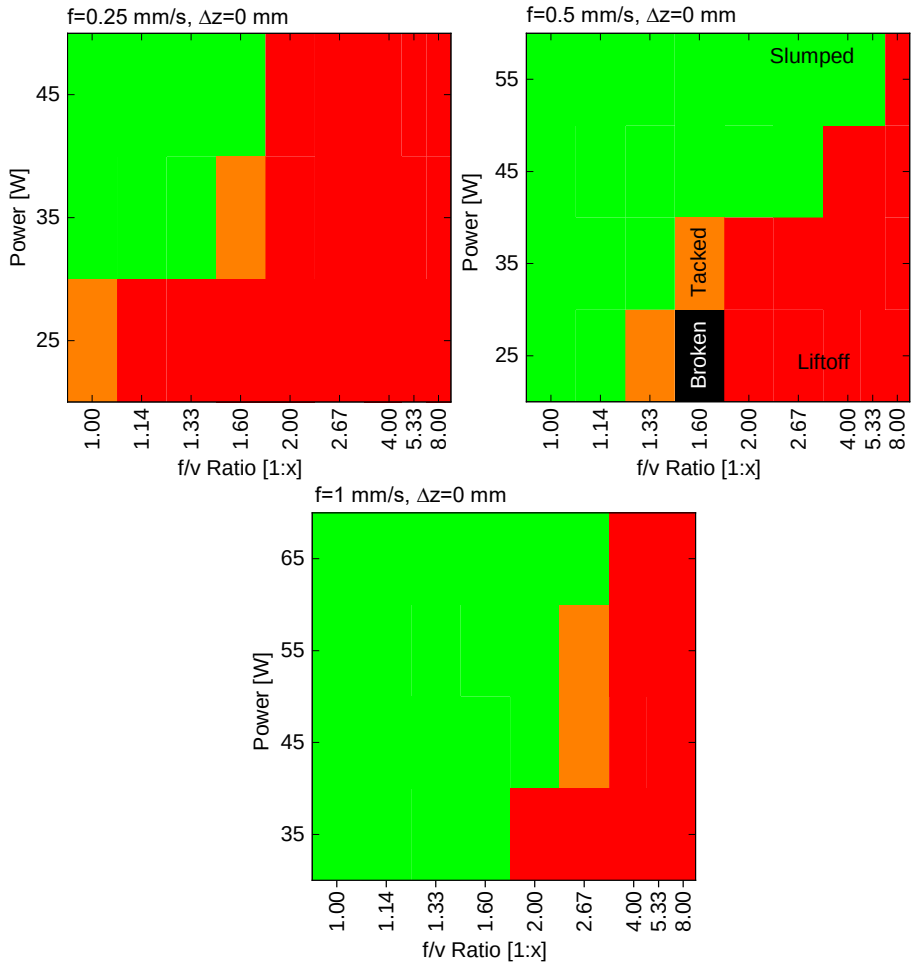

Figure 4: Process maps relating the input *f*/v ratio and input laser power to the resulting track morphology for a few filament feed rates.

3. Incorporating shift in Δz

Observing this liftoff failure mode further, it appears that once the filament disconnects from the substrate, the deposition will stabilize printing horizontally at some distance above the substrate z_{Error}, as shown in Fig 5 below. This prompted an expansion of the process zone by including a new printing parameter Δz, representing the upward shift in the substrate to correct for this height error. This was done empirically by repeating the same process zone above (f = 0.5 mm/s), sweeping Δz and f/v over a few powers. The process zones for these experiments, shown below in Fig 6, show a significant increase in the viable f/v ratios available, with the higher power process zones reaching the desired ratio of 1/16. It is worth noting that at very high laser powers (and sufficiently slow scan speeds), the surface of the deposited glass can overheat, vaporizing important interstitial ions and altering the material properties. At f/v = 1/16, vaporization is minimized due to the increased scan rate. However, this effect places an upper limit on the input power that can be used for depositions. Additionally, at the highest laser powers at slower feed rates, the filament can get so hot that the molten connection to the substrate becomes unstable, resulting in a disconnection between the materials where the filament balls up (noted in Fig 6).

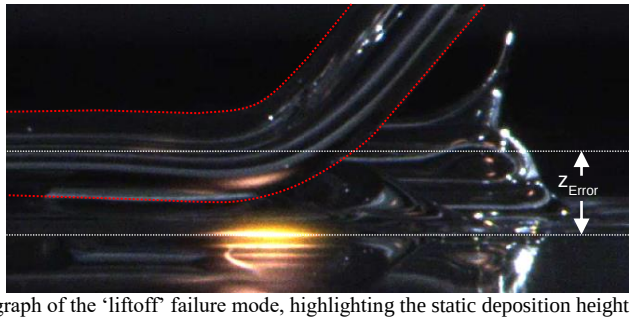

Figure 5: Photograph of the 'liftoff' failure mode, highlighting the static deposition height off the substrate.

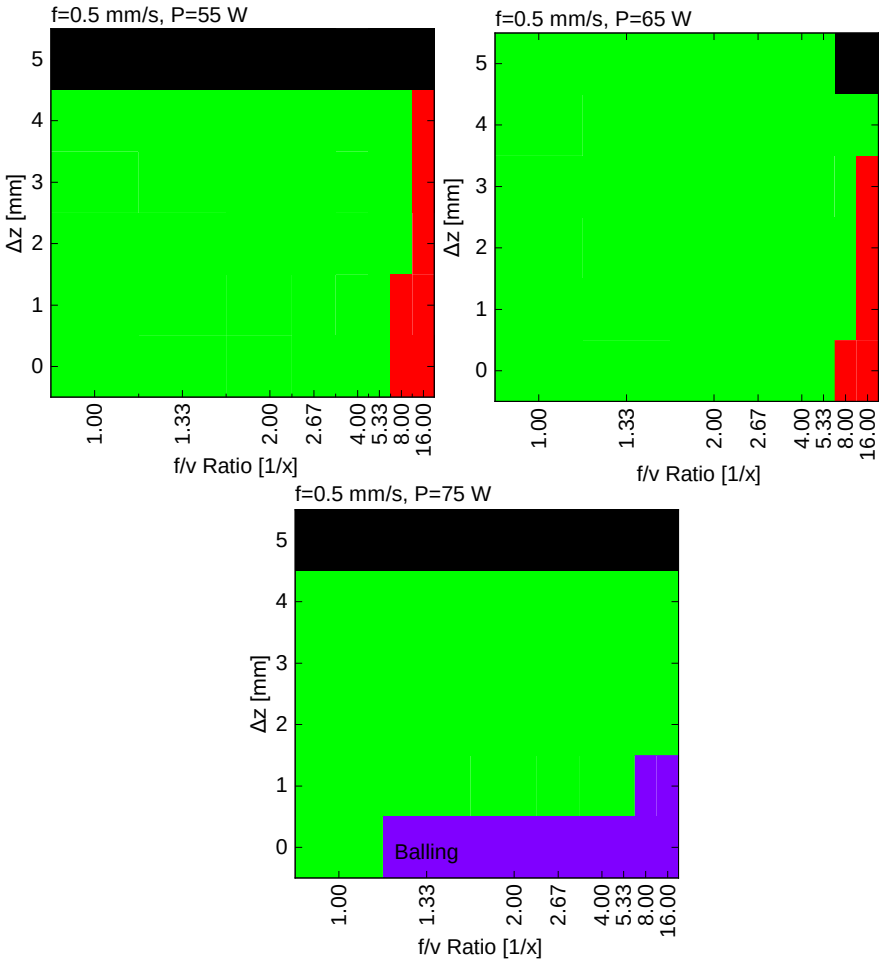

Figure 6: Results of the expanded process zone, incorporating Δz.

The significant increase in the viable *f/v* ratios can be explained by examining how the shift in Δz affects the temperature and loading profiles of the bead. Conceptually, the deposition behavior of the glass is determined by the temperature of the interface between the filament and substrate (illuminated by the laser), as well as the temperature on the opposite side of the filament. In short, the temperature at the interface must be sufficiently high to allow the filament and substrate to coalesce into a single piece of material. Additionally, the back surface must be warm enough to allow the filament to bend but still be cool enough to apply force from the feeder to the melt pool. To capture the temperature in these two areas, an infrared camera (Optris PI 640) was used in the directions indicated by Fig 7a below. As shown, when measuring the interface temperature, the maximum temperature of the viewing area is extracted, while on the back surface, an average temperature of a 5 px ×5 px area is extracted. The smaller defined area on the back surface of the filament is used to distinguish the bending point from the rest of the image, compared to the interface temperature, which is the hottest point of the deposition. Figure 7b shows the effect of

changes in *f/v* on the temperature profile as solid lines (Δ*z*=0). These data points were repeated for a shift of Δ*z*=2 mm, shown as dashed lines in the image. As shown in the left figure, there is very little temperature shift on the front surface by changing Δz (much more sensitive to *P* and *f/v*). However, on the back surface, there is a significant decrease in the back surface temperature when increasing Δ*z*. This decreased back surface temperature may explain why depositing at a shifted z-plane allows for higher *f/v* ratios, as the cooler (and therefore stiffer) back surface can re-apply the force from the filament feeder onto the melt pool.

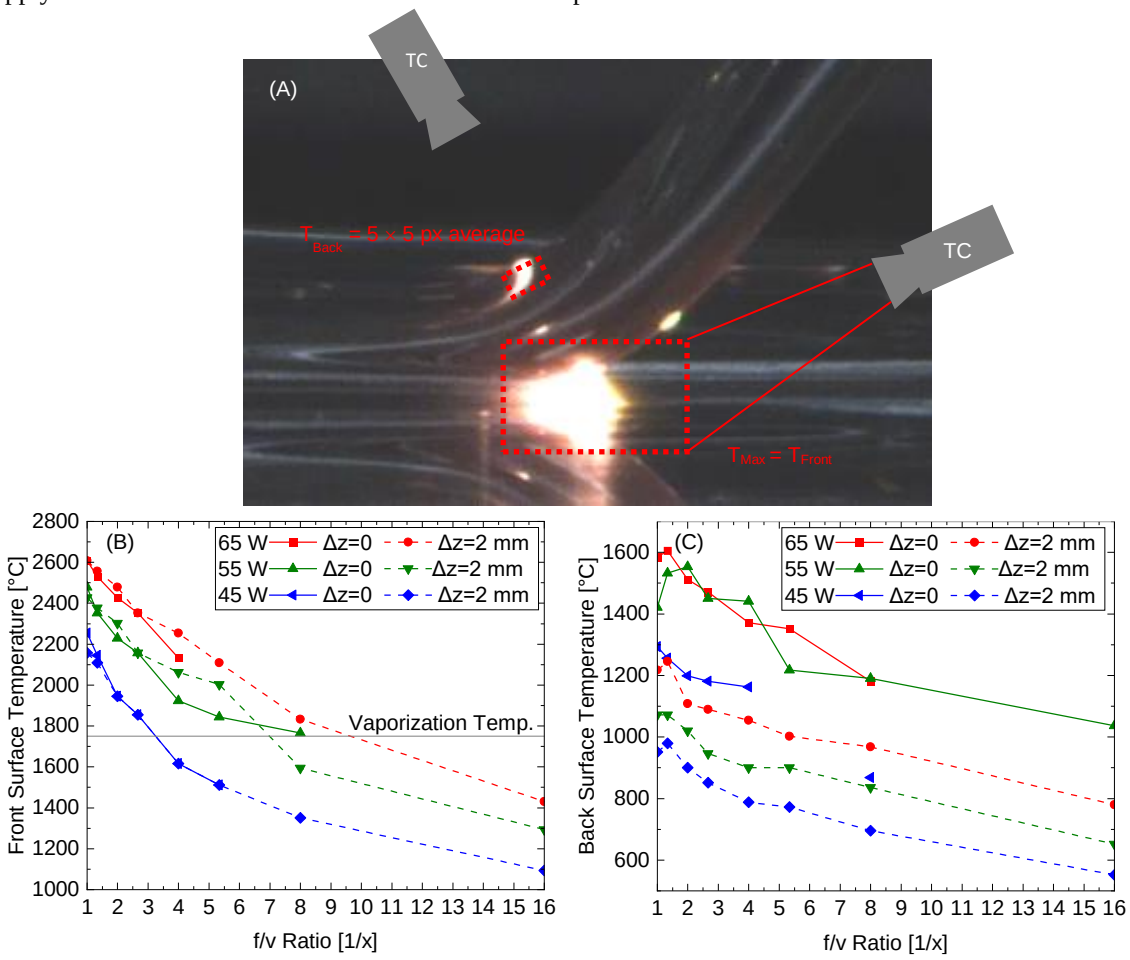

Figure 7: (A) Diagram of how the front and back surface temperatures were captured with the thermal camera. (B-C) Front and back surface temperatures are plotted as a function of *f/v* ratio, laser power, and Δz, respectively.

4. Effect of Feed Rate

Expanding the process zone to include other feed rates can significantly alter the viable process zone and deposition mechanics. For instance, the data set for the *f* = 0.25 mm/s (See Fig. 8 below) has a significantly larger portion of the process zone fail via balling the filament. Heat has more time to diffuse through the filament cross-section at these lower feed rates, resulting in a much more uniform temperature profile. This much hotter back surface temperature reduces the force the feeder can deliver to the melt pool. However, in this deposition mode, the surface tension of the melt pool supplies the adhesion force between the two pieces (as highlighted by the necking behavior seen in Fig 8b).

Increasing the feed rate to *f*=0.75 mm/s results in the opposite effect, decreasing the time for heat to diffuse to the back surface, resulting in a larger temperature difference. The process maps between *f* = 0.75 mm/s (See Fig 10) and *f* = 0.5 mm/s are not significantly different, due to the similar deposition modes, but due to the higher base feed rates, more laser power must be used.

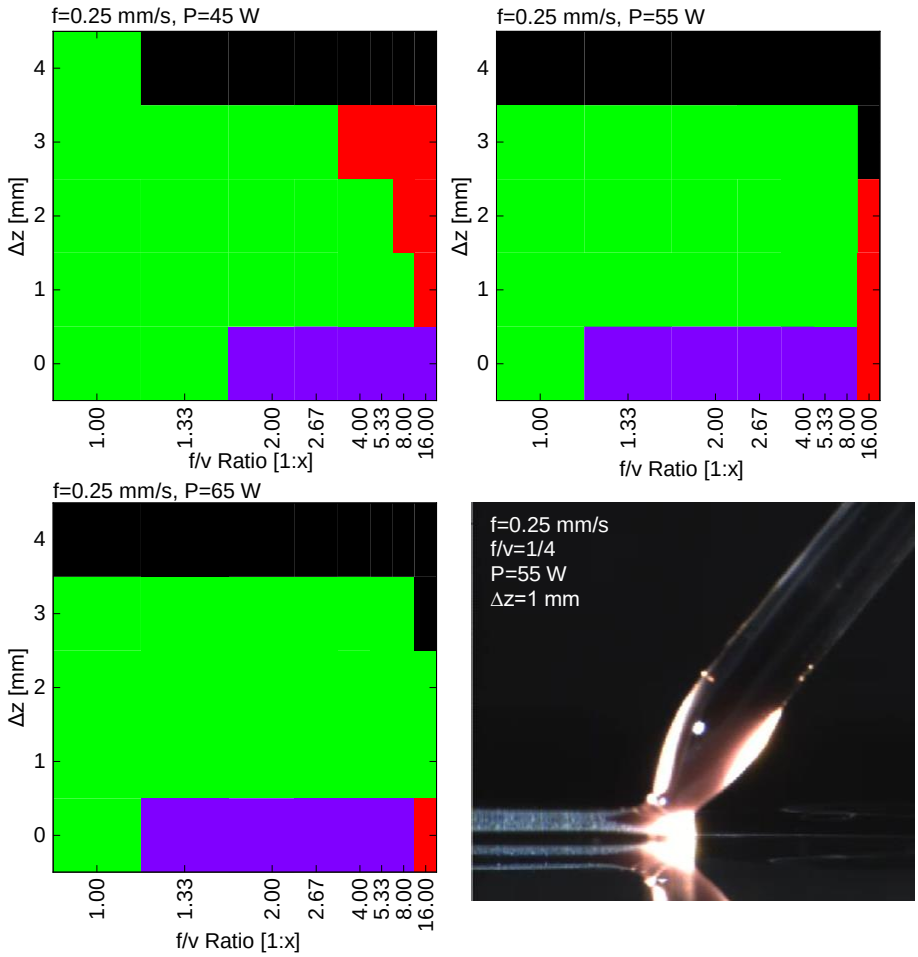

Figure 9: Process maps for the baseline feed rate *f*=0.25 mm/s at different parameters, (Bottom right) example photograph of deposition at low feed rates, showing significant necking on both sides of the filament characteristic of surface tension driven deposition.

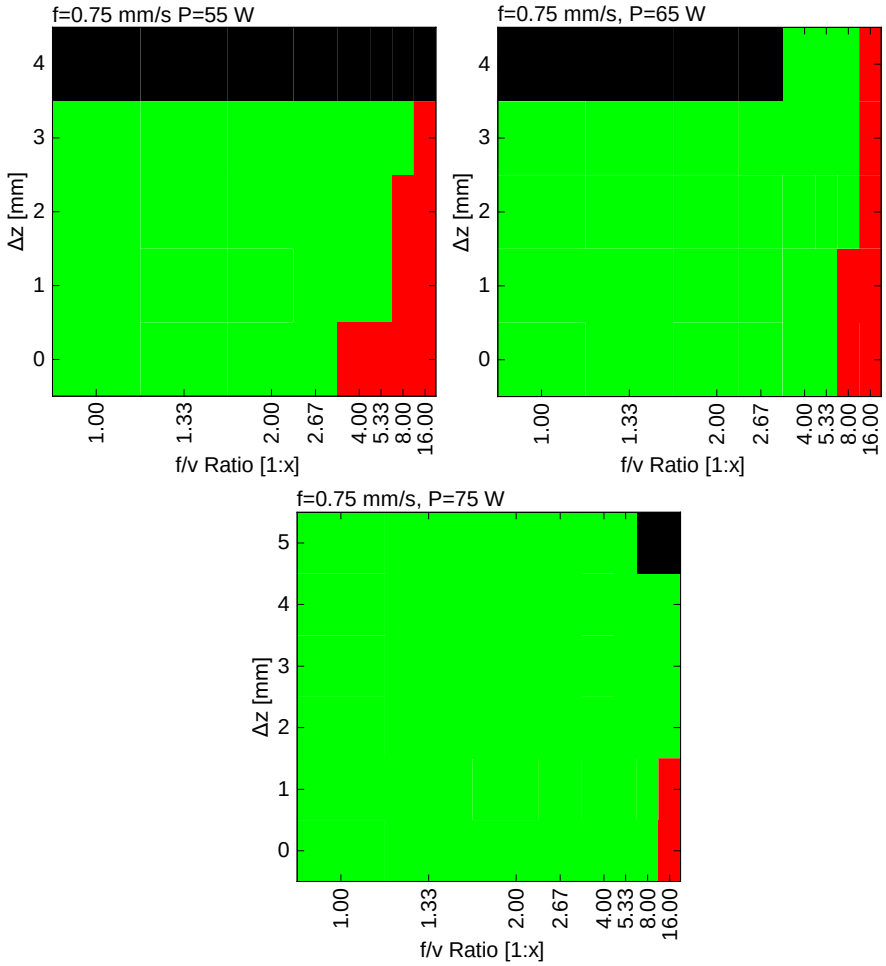

Figure 10: Process maps at *f*=0.75 mm/s deposition rate.

5. Application Space

Using the parameter space defined above for f = 0.5 mm/s, some example pieces were created to showcase the effects of underfeeding the filament during deposition. As shown in Fig 11 below, altering the *f/v* ratio from 1 (left) to 1/4 (right) shows a significant decrease in layer height, for example variable radius vase structure, from 1.25 mm to 0.45 mm. Transitioning from straight-line depositions to creating complex vase shapes is non-trivial due to additional failure modes and challenges with identifying the correct layer height for the depositions, requiring further work to address these challenges. While the *f/v* ratio is not close to the 1/16 target, for this example, we have decreased the equivalent filament radius by half and the layer height by almost 65%.

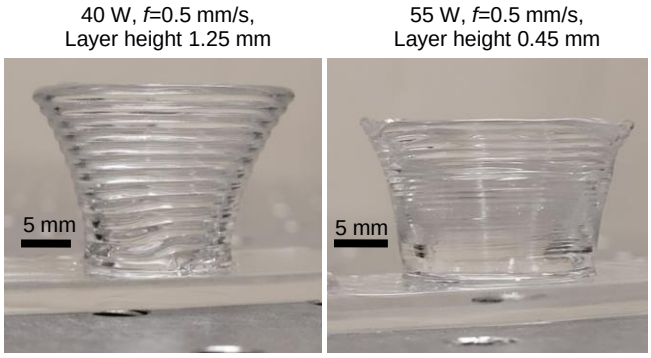

Figure 11: Comparison of *f/v*=1 (Left) and *f/v=1/4* vases (Right)

While a decrease in layer height for artistic vase pieces is useful for demonstration purposes, the technical application space that this technique would be most useful for is in the creation of optical forms, using the decreased layer height to approach the near-net shape more accurately for a lens. As shown in the solid cylindrical pyramid shapes below, there is a significant reduction in the surface variation between the *f/v*=1 and *f/v*=1/4 shapes, requiring less laser polishing and secondary post-processing to produce the final desired shape. This reduction of surface variation is visible in the photographs but most easily identified by viewing the structure profile created from a 3D scan of the pieces (bottom of Fig 12).

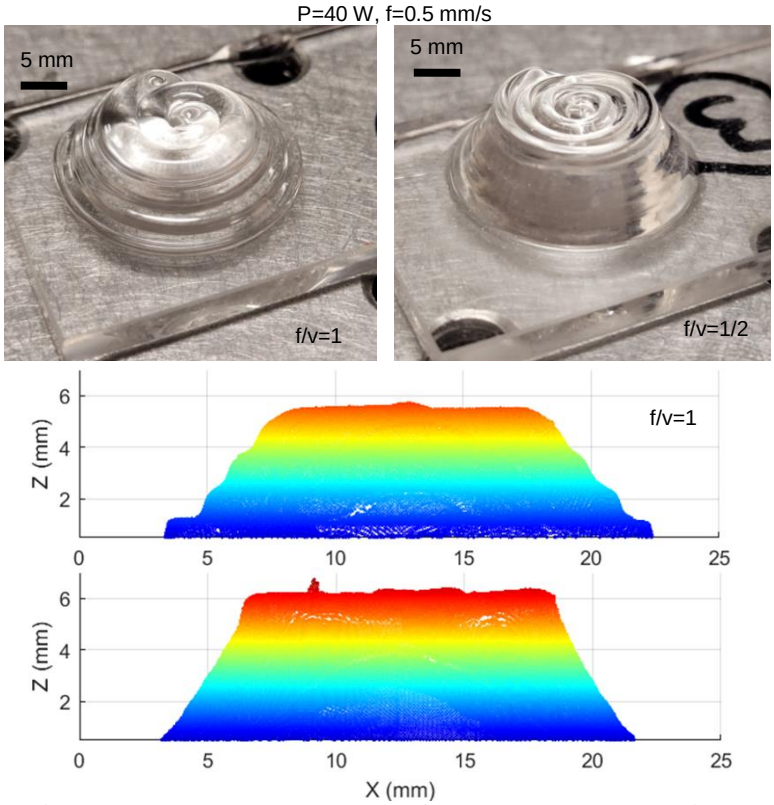

Figure 13: (Top) Photographs of solid cylindrical pyramid structures at two *f/v* ratios. (Bottom) Side-view of 3D height map scans of structures (color maps to height of data point)

6. Conclusions

The Digital Glass Forming method has shown the ability to deposit complex 3D glass volumes as fully dense pieces and as sparse freestanding structures. The resolution of this process is limited by the input feedstock diameter, and the high molten viscosity of glass presents challenges for extrusion methods for diameter reduction. Taking inspiration from fiber drawing techniques, the filament is underfed relative to the table scan speed during deposition, but the minimum draw ratio (*f/v* = 0.2) is limited by a failure mode where the filament lifts off the substrate, stabilizing at some static z_{Error} height above the substrate. By shifting the substrate upwards by a Δz value, this error can be corrected for, allowing for draw ratios as high as *f/v*=1/16 for straight-line tracks. Altering the Δz value results in a difference in the temperature profile of the melt pool, maintaining the front surface temperature but decreasing the back surface temperature significantly. This decrease in back surface temperature (increase in stiffness) allows the filament to deliver force more effectively from the filament feeder to the melt pool, keeping the filament on the substrate. It is worth noting that the target ratio is not the physical limit of the deposition, only an arbitrary target for this experiment set. Future works on this method will be focused on identifying the physical limits on *f/v* ratio (e.g., Rayleigh instability or limits in the heat diffusion rate). Additionally, there is a need to estimate the melting pool's loading force as a function of input parameters and explore additional parameter spaces, such as using a different initial feedstock diameter (e.g., 1 mm OD filaments or 125 µm optical fiber).

7. References

[1] Kreidl, N., Recent applications of Glass Science, *J. Non-Cryst. Solids* 123, (1990)

[2] Hülsenberg, D., Harnisch, A., Bismarck, A., [Silicate Glasses: A Class of Amorphous Materials. In: Microstructuring of Glasses. Springer Series in Materials Science, Vol 87.] Springer, Berlin, Heidelberg. (2008)

[3] Marchelli, G., Prabhakar, R., Storti, D., Ganter, M., The guide to glass 3D printing: developments, methods, diagnostics, and results *Rapid Prototyp. J.* **17**(3), (2011)

[4] Kotz, F., Arnold, K., Bauer, W., Schild, D., Keller, N., Sachsenheimer, K. Nargang, T., Richter, C., Helmer, D., Rapp, B. E., Three-dimensional printing of transparent fused silica glass, *Nature*, 544 (2017)

[5] Wang, H-R., Cima, M. J., Kernan, B. D., Sachs, E.M. Alumina-doped silica gradient-index (GRIN) lenses by slurry-based three-dimensional printing (S-3DP^{TM}), *J. Non-Cryst. Solids*,349, (2004)

[6] Destino, J. F. et. al, 3D Printed Optical Quality Silica and Silica-Titania Glasses from Sol-Gel Feedstocks, *Adv. Mater. Technol*, 3, (2018)

[7] Klein, J., Stern, M., Franchen, G., Kayser, M., Inamura, C., Dave, S., Weaver, J.C., Houk, P., Colombo, P., Yang, M., Oxman, N., 2015 "Additive Manufacturing of Optically Transparent Glass" 3D Print. and Add. Mfct. 2(3), pp. 92-105

[8] Gal-Or, E., et al "Chemical analysis using 3D printed glass microfluidics" Anal. Methods, 11, 1802–1810, (2019)

[9]Witzendorff, P., Pohl, L., Suttmann, O., Heinrich, P., Heinrich, A., Zander, J., Bragard, H., Kaierle, S., "Additive manufacturing of class: CO_2-Laser glass deposition printing" *Procedia CIRP 74*, 272-275, (2018)

[10] Liu, C., Oriekhov, T., Fokine, M., "Investigation of glass bonding and multi-layer deposition during filament-based 3D printing" *Front. Mater.* 9:978861, (2022)

[11] Kranert, F., Rettschlag, K., Wienke, A., Hohnholz, A., Neumann, J., Kracht, D., Lachmayer, R., "Generation of functional curved waveguides by CO_2-laser based deposition of coreless fused silica fibers" *Proc. Of SPIE Vol. 11349* (2020)

[12] Capps, N., Zhu, C., Goldstein, J., Kinzel, E., "Digital Glass forming of Photonics" *Opt. Eng.* **62**(7), (2023)

[13] Peters, D., Drallmeier, J., Bristow, D., Landers, R., Kinzel, E., "Sensing and control in glass additive manufacturing" *Mechatronics* 56 188-197, (2018)

[14] Blalock, T., Medicus, K., Nelson, J., "Fabrication of freeform optics" *Opt. Manuf. and Testing XI* (2015)

[15] Tian, W., Chiu, W., "Temperature prediction for CO_2 laser heating of moving glass rods" *Opt. Laser Technol.* **36** (2004)

[16] Capps, N, Goldstein, J., Rettschlag, K., Sleiman, K., Jaeschke, P., Kaierle, S., Kinzel, E., "Digital laser heating of the filament / substrate interface in digital glass forming" *Manuf. Letters* **31** (2022)

[17] Spinner, S., Napolitano, A., "Further Studies in the Annealing of a Borosilicate Glass" *J. Res. Natl. Bur. Stand. A Phys. Chem.* **70,** (1966)

[18] Ebendorff-Heidepriem, H., Monro, T., "Analysis of glass flow during extrusion of optical fiber preforms", *Opt. Mater. Express* **305** (2012)

[19] Liu, S., Banta, L., "Parametric Study of Glass Fiber Drawing Process" *Int. J. Appl. Glass Sci.* **1** (2010)